Facies-constrained FWI: Toward application to reservoir characterization

Nishant Kamath[1], Ilya Tsvankin[2], and Ehsan Zabihi Naeini[3]

Abstract

The most common approach to obtaining reservoir properties from seismic data exploits the amplitude variation with offset response of reflected waves. However, structural complexity and errors in the velocity model can severely reduce the quality of the inverted results. Full-waveform inversion (FWI) has shown a lot of promise in obtaining high-resolution velocity models for depth imaging. We propose supplementing FWI with rock-physics constraints obtained from borehole data to invert for reservoir properties. The constraints are imposed by adding appropriately weighted regularization terms to the objective function. The advantages of this technique over conventional FWI algorithms are shown by conducting synthetic tests for both isotropic and VTI (transversely isotropic with a vertical symmetry axis) models. The medium parameterization for FWI is selected using radiation (scattering) patterns of perturbations in the model parameters.

Introduction

Most conventional reservoir-characterization techniques operate with the amplitude variation with offset (AVO) response of reflected waves and are typically applied in the migrated domain. Such "classic" methods invert the AVO signature in deterministic or stochastic fashion either for elastic parameters or directly for reservoir properties (Russell, 1988). For example, Coléou et al. (2005) propose an approach whereby the difference between synthetic gathers, generated for an initial petroelastic model, and migrated recorded data is iteratively reduced by model updating. The inversion yields more plausible reservoir parameters by incorporating prior information about geologic facies (Saussus and Sams, 2012). Such information can be included in the form of linear relationships between elastic properties of each facies (e.g., between acoustic impedance and density). Conventional techniques, however, suffer from several inherent problems; in particular, the quality of migrated gathers depends on the accuracy of the velocity model, and inversion uses only reflection amplitudes (rather than waveforms).

Full-waveform inversion (FWI) estimates subsurface properties (such as velocity, impedance, anisotropy parameters, etc.) directly from recorded seismic traces. The inverse problem is highly nonlinear and overdetermined yet underconstrained. There are inherent trade-offs between model parameters, which cannot be resolved independently using just the data misfit (Alkhalifah and Plessix, 2014; Kamath and Tsvankin, 2016). Incorporating facies-based and other constraints sets bounds in the model space and helps obtain more accurate and geologically plausible results (Asnaashari et al., 2013; Duan and Sava, 2016; Zabihi Naeini et al., 2017).

In this paper, we incorporate prior information about geologic facies into the FWI objective function. The technique is first applied to purely isotropic and then to VTI (transversely isotropic with a vertical symmetry axis) elastic models. We demonstrate the advantages of the facies-based approach (compared to the standard FWI) and discuss the influence of parameterization on the inversion results. In the presence of anisotropy, our method takes advantage of prior information to resolve VTI parameters, which are otherwise poorly constrained.

Although the models considered in the following are not structurally complicated, the classic AVO-based methods could still produce erroneous results. In particular, failing to properly account for anisotropy, amplitude distortions related to mode conversions, or the presence of multiples could substantially degrade estimation of reservoir parameters.

Methodology

FWI is an inversion method that usually operates with raw seismic data (e.g., shot records) and generally aims to use the entire waveforms including different wave types. The output depends on the specific formulation of the problem and study objectives (which also determine the choice of forward modeling) and can include parameters of acoustic or elastic (possibly anisotropic) models. To apply FWI as a reservoir-characterization tool, one can follow the workflow in Figure 1 discussed by Zabihi Naeini et al. (2016, 2017).

In its most general form, FWI is performed by minimizing an objective function which typically represents the l_2 norm of the difference between the modeled and recorded data (i.e., data misfit). Here, we propose to apply model constraints by including additional terms in the objective function $E(\mathbf{m})$:

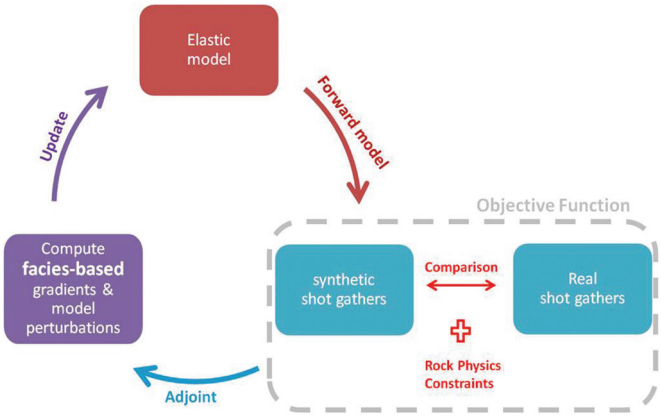

Figure 1. Concept diagram of anisotropic elastic reservoir-oriented FWI (adapted from Zabihi Naeini et al., 2016).

[1]Formerly Colorado School of Mines; presently Université Grenoble Alpes.
[2]Colorado School of Mines.
[3]Ikon Science.

https://doi.org/10.1190/tle36110924.1.

$$E(\mathbf{m}) = \left\|\mathbf{W}_d\left(\mathbf{d}_m(\mathbf{m}) - \mathbf{d}_o\right)\right\|^2 + \beta\left\|\mathbf{W}_m\left(\mathbf{m} - \mathbf{m}_c\right)\right\|^2 = E_d(\mathbf{m}) + E_{\text{prior}}(\mathbf{m}), \quad (1)$$

where $\mathbf{m}$ is the vector of model parameters, $\mathbf{d}_m(\mathbf{m})$ denotes data generated for model $\mathbf{m}$, $\mathbf{d}_o$ is the observed data, $\mathbf{m}_c$ is the model constraints presumably obtained from borehole information, $\mathbf{W}_d$ and $\mathbf{W}_m$ are the data- and model-weighting matrices, respectively, and β determines the relative contribution of prior information. We apply the weighting matrices in the form of masks, which selectively update certain facies in the model.

The first term $[E_d(\mathbf{m})]$ in equation 1 represents the data misfit and the second one $[E_{\text{prior}}(\mathbf{m})]$ is the model misfit, which includes rock-physics constraints for each facies. The constraints are in the form of linear relationships between different model parameters. By referring to "standard" FWI in the following, we mean the result of minimizing only the data misfit $E_d(\mathbf{m})$ (i.e., $\beta = 0$).

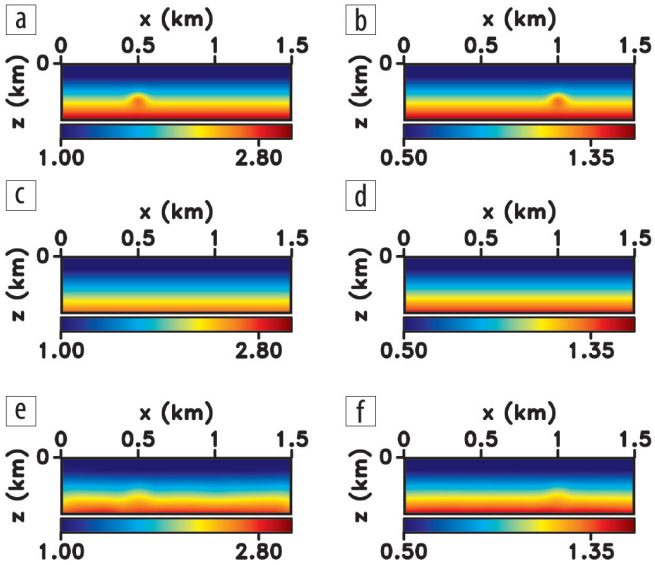

Figure 2. Elastic isotropic FWI of diving P- and SV-waves. The actual velocities (a) V_P and (b) V_S, the initial (c) V_P and (d) V_S, and the inverted (e) V_P and (f) V_S. The velocities here and in the subsequent plots are in km/s.

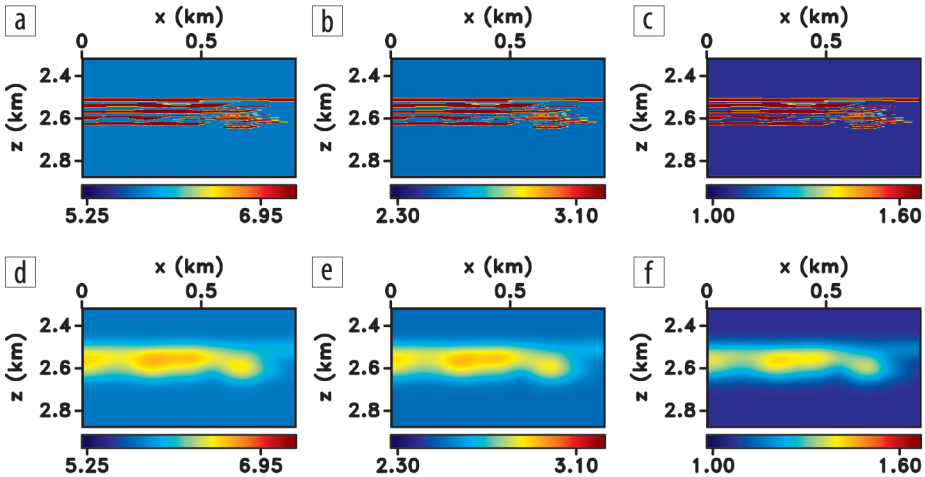

Figure 3. Two-facies isotropic model parameterized by the (a) impedance I_P and the velocities (b) V_P and (c) V_S. The initial parameters (d) I_P, (e) V_P, and (f) V_S. The P-wave impedance is in 10^{-6} kg/(m^{2}s).

Representative facies are supposed to be identified from well data. We incorporate model constraints $[E_{\text{prior}}(\mathbf{m})]$ into FWI one facies at a time. The inversion algorithm, designed for elastic VTI media, is described in Kamath and Tsvankin (2016). The wavefield is generated using time-domain finite-difference modeling, and the gradient of the data misfit with respect to the model parameters is computed from the adjoint-state method (Plessix, 2006; Kamath and Tsvankin, 2016). The bounded, low-memory Broyden-Fletcher-Goldfarb-Shanno (BFGS) algorithm of Byrd et al. (1995) is employed to update the model at each iteration.

Numerical experiments

Isotropic models. When performing FWI, it is common to first invert diving-wave arrivals to update the background velocity model. Here, we show an example of inverting such data for a simple isotropic model with vertical gradients and Gaussian anomalies in the P- and S-wave velocities, V_P and V_S (Figure 2). The initial V_P- and V_S-fields (Figures 2c and 2d, respectively) have substantially lower gradients compared to the actual model. P- and S-wave transmission (in this case, diving wave) data are influenced by V_P and V_S, respectively, with no trade-offs between the velocities (Kamath and Tsvankin, 2016). Hence, the inversion algorithm is able to update both V_P and V_S and partially recover the Gaussian anomalies. The quality of the inversion results depends on the magnitude of the velocity gradients and the maximum offset-to-depth ratio. Note that for the model in Figure 2 the maximum offset is about three times larger than the section thickness.

Once the background velocities have been updated, one can incorporate reflection data to further refine the model. We use a two-facies isotropic model (Figure 3), parameterized in terms of the P-wave acoustic impedance I_P in addition to the velocities V_P and V_S, to test two different facies-constrained techniques. The initial model is obtained by smoothing the actual impedance and velocity fields.

To assess possible parameter trade-offs, it is convenient to analyze so-called radiation (scattering) patterns (Operto et al., 2013; Alkhalifah and Plessix, 2014; Kamath and Tsvankin, 2016). The P-wave radiation patterns yield an estimate of the P-wave energy scattered by a secondary source (i.e., by an anomaly in a model parameter) as a function of opening angle (Figure 4). Parameterizing the model in terms of I_P, V_P, and V_S (Figure 4a) ensures that small-offset reflection data are controlled primarily by I_P, whereas V_P influences P-wave diving energy. Still, there are trade-offs between V_P and V_S at intermediate opening angles, although the P-wavefield is generally influenced more by V_P (whose radiation pattern has a larger magnitude) than V_S.

Technique I. We apply a two-stage process by first running FWI without any model constraints (Figures 5a–5c). From the obtained inversion results we

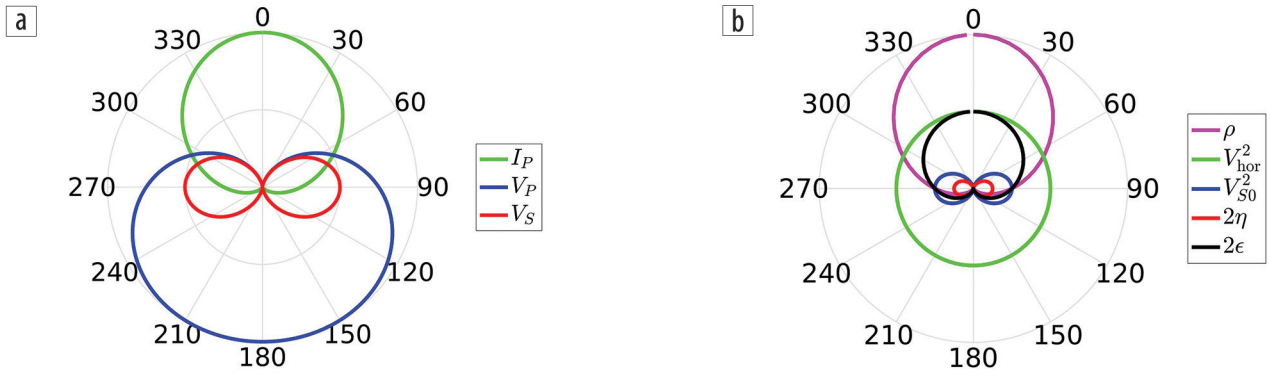

Figure 4. P-wave radiation patterns for (a) an isotropic model parameterized in terms of the P-wave impedance, I_P, and P- and S-wave velocities, V_P and V_S; and (b) a VTI model parameterized in terms of the squared velocities V_{hor} and V_{S0}, the anisotropy coefficients ϵ and η, and density.

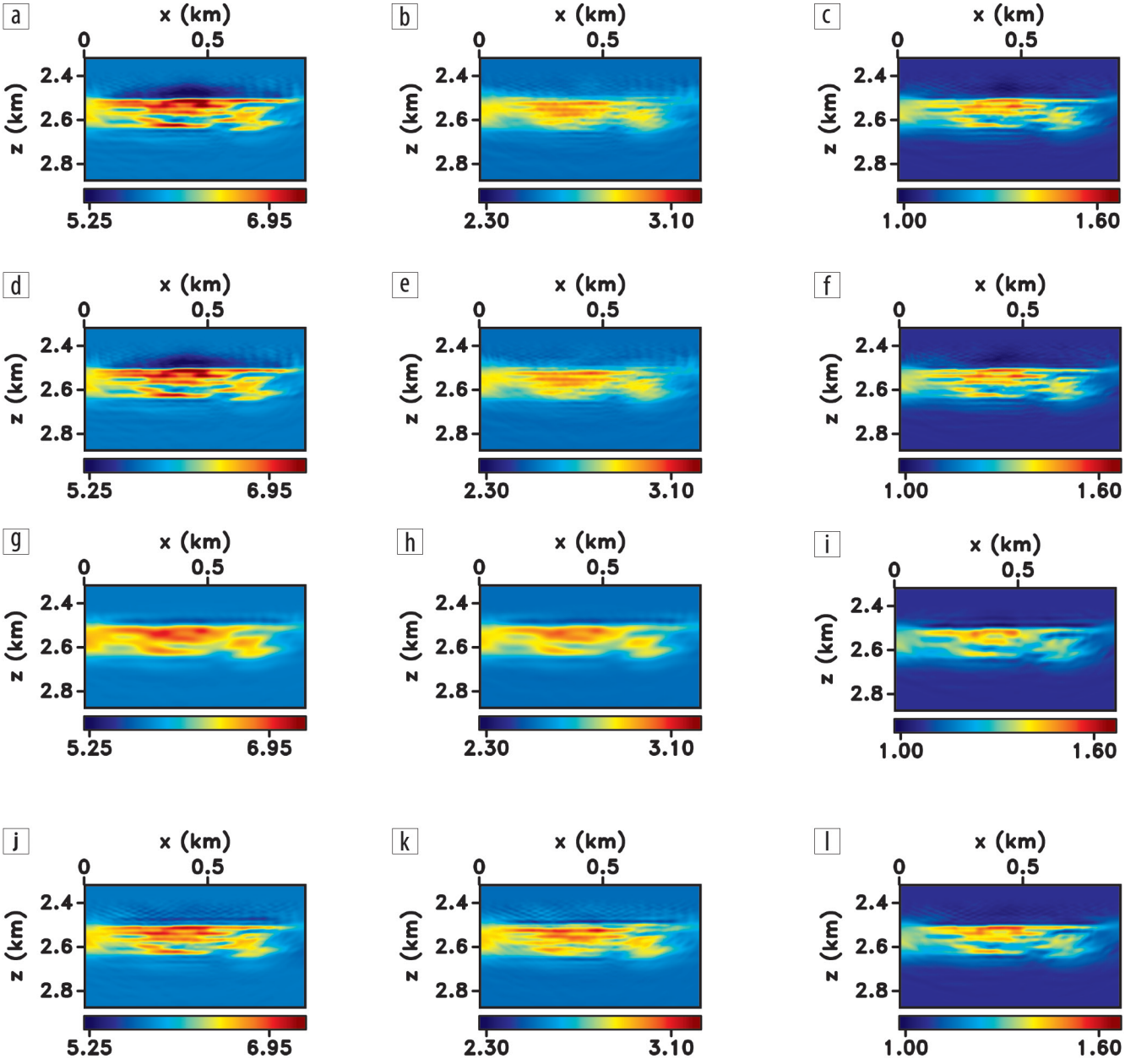

Figure 5. Inverted parameters (a) I_P, (b) V_P, and (c) V_S from the first stage of the facies-based inversion (technique I). The parameters (d) I_P, (e) V_P, and (f) V_S from the second inversion stage (technique I). The results for technique II: the parameters (g) I_P, (h) V_P, and (i) V_S from the first inversion stage and (j) I_P, (k) V_P, and (l) V_S from the second stage.

compute the ratios I_P/V_P and I_P/V_S for every grid point in the model. It is assumed that the exact values of I_P/V_P and I_P/V_S are known for each facies (e.g., from well logs). Each grid point in the model is assigned to one of the facies depending on how close the inverted ratios are to the actual values, thereby yielding the model constraints in Figure 6. At the second inversion stage, we perform facies-based FWI by imposing these constraints (i.e., by adding $E_{prior}(\mathbf{m})$ in equation 1). There is an improvement in the resolution of all three inverted parameters, most notably in the V_S field (compare Figures 5c and 5f).

Whereas we compute the constraints by assigning each grid point in the model to a specific facies, further improvement could be achieved by treating each grid point as a weighted average of all facies (Zhang et al., 2017). The weights can be computed from an assumed parameter distribution (e.g., Gaussian), and this procedure can be incorporated into the inversion to allow for updates in the constraints themselves.

Technique II. An alternative approach is to perform the inversion by using the values of I_P/V_P and I_P/V_S assumed to be known a priori (in practice, from well data) in the first layer as constraints on the velocities V_P and V_S (Figures 5g–5i). The output produces the initial model for the next inversion stage, in which the model constraints (the ratios I_P/V_P and I_P/V_S from the second facies) are imposed only on the second layer. This is done by applying a mask ($\mathbf{W}_m$ in equation 1) constructed using the results of the first inversion stage. This mask produces weights equal to unity between depths of 2.45 and 2.7 km and zero elsewhere. In addition, at the second stage we include higher temporal frequencies in the data. The results obtained by the facies-based approach (Figures 5j–5l) are clearly superior to those of the standard FWI.

The parameters I_P and V_P are better resolved using technique II than technique I. The artifacts in the inverted impedance I_P at depths close to 2.5 km are significantly reduced (compare Figures 5d and 5j). Technique II also produces larger updates in the velocity V_P, which yields a more accurate V_P field. The shear-wave velocity V_S obtained by technique I, however, has larger wavenumbers and, hence, higher resolution. Because the overall performance of technique II is better, we employ a similar approach for the subsequent tests.

For the next experiment, we use another isotropic model with a thin laterally heterogeneous reservoir located at a depth of 1.6 km beneath a stratified overburden (Figure 7). The lateral variation of the elastic properties within the reservoir is created by interchanging oil, gas, and brine sands. The facies encasing the reservoir represents shale; there is a total of three nonreservoir facies in the model.

As before, we proceed in two stages: first, the I_P/V_P and I_P/V_S ratios for the shale facies are employed as constraints for depths between 1.1 and 2.3 km. The mask used to impose the constraints is displayed in Figure 8a. The results of this stage are used as the input for the next one, in which the constraints are applied just to the reservoir facies.

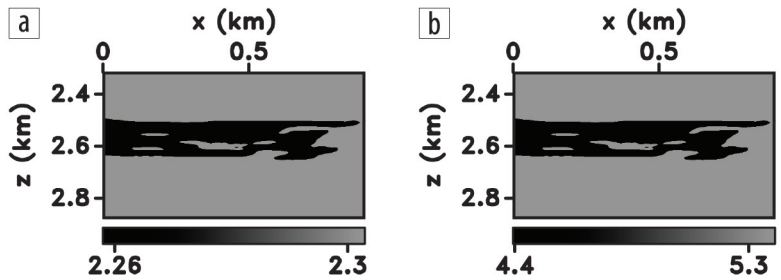

Figure 6. Model constraints on the ratios (a) I_P/V_P and (b) I_P/V_S (in g/cm³) obtained from the respective actual values and those computed from the I_P, V_P, and V_S fields in Figures 5a–5c.

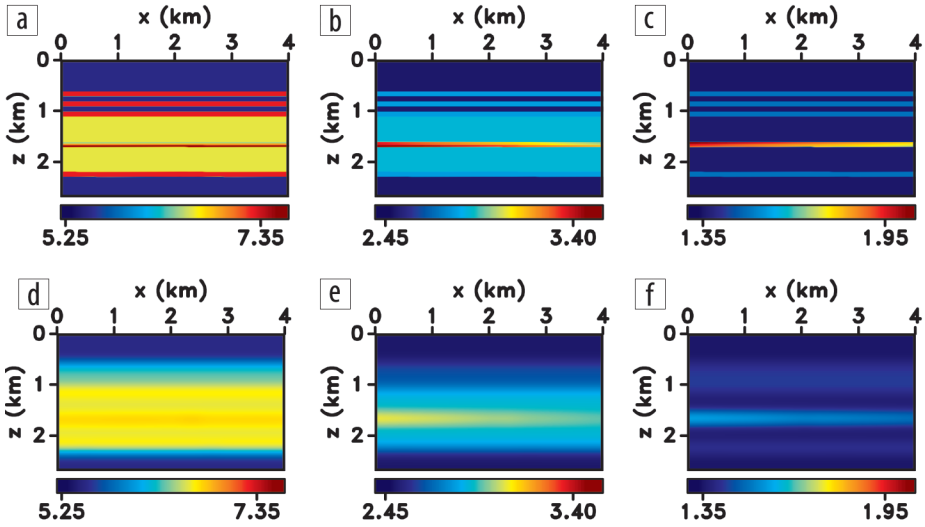

Figure 7. Isotropic model described by the (a) acoustic impedance (AI) and the velocities (b) V_P and (c) V_S. The initial parameters (d) AI, (e) V_P, and (f) V_S.

Starting from the initial model in Figures 7d–7f, the standard FWI produces the I_P- and V_P-fields with some artifacts in the shale facies (Figures 9a–9c). In addition, the reservoir layer is not sufficiently well resolved. The shale parameters obtained after the first stage of our facies-based inversion are more consistent with the actual model (Figures 9d–9f). The reservoir layer, however, exhibits artifacts similar to those in the standard FWI. The second stage of the facies-based inversion mitigates these distortions, especially in the I_P and V_P fields (Figures 9g–9i). However, the density field computed from the inverted acoustic impedance and P-wave velocity is not sufficiently accurate. This is most likely because the inverted I_P field has a higher vertical resolution compared to that of the velocity V_P.

VTI model. It is generally well recognized that reservoir-oriented FWI has to take anisotropy into account (Zabihi Naeini et al., 2016). We extend the proposed method to elastic VTI media as the first step toward incorporating realistic anisotropic symmetries. The parameterization includes V_{hor} (the P-wave horizontal velocity), V_{S0} (the S-wave vertical velocity), and the anisotropy

coefficients ϵ and $\eta \equiv (\epsilon - \delta) / (1 + 2\delta)$. This choice, suggested by radiation-pattern analysis (Alkhalifah and Plessix, 2014; Kamath et al., 2016), helps obtain superior results for V_{hor} because it influences P-wave energy uniformly for all incidence angles (Figure 4b). In addition, it optimizes the inversion by reducing parameter trade-offs. Indeed, although both V_{hor} and ϵ influence P-wave energy at small opening angles, for larger angles there is almost no trade-off between V_{hor} and the other parameters.

The VTI model in Figure 10 has the same vertical velocities V_{P0} and V_{S0} and density as the isotropic model in Figure 7. (Here and in the following figures, we display the P-wave horizontal velocity V_{hor} rather than the vertical velocity V_{P0}.) However, we consider the encasing shale to be VTI (typical symmetry for shales), while the reservoir sand is isotropic, which helps differentiate between them in the inversion. Because we were unable to properly update the density for isotropic models, the actual density field is smoothed and kept fixed during the inversion. The smoothing filter employed to generate the initial velocity models is also used to obtain the initial anisotropy parameters η and ϵ, as well as the density (which is not updated).

We invert for the four model parameters (V_{hor}, V_{S0}, η, and ϵ) using both the standard FWI and our facies-based approach. The standard algorithm (which computes the inversion gradient just of the data misfit) produces large artifacts in the inverted η- and ϵ-fields between depths of 0.5 and 1 km (Figures 10k and 10l). The distortions are caused by the trade-offs between the P-wave horizontal velocity V_{hor} and the anisotropy coefficients η and ϵ (Figure 4b). In addition, the lower sensitivity of the objective function to the parameter η leads to its insufficient updates inside the reservoir.

To carry out facies-based inversion for this model, we first impose "isotropic" constraints (i.e., penalize nonzero values of η and ϵ by employing the mask in Figure 8b) on the reservoir. The scaling factor β from equation 1 is chosen such that the root mean square values of the inversion gradients with respect to $E_d(\mathbf{m})$ and $E_{prior}(\mathbf{m})$ are comparable. The velocities V_{hor} and V_{S0} are generally well constrained (Figures 10m and 10n), with our facies-based method producing a slight improvement over the standard FWI inside the reservoir. The coefficient ϵ is also accurately estimated by both methods (Figures 10l and 10p) with positive values for the shale, whereas the reservoir is practically isotropic ($\epsilon \approx 0$). The facies-based inversion, however, results in significant improvements in the η estimates inside the reservoir.

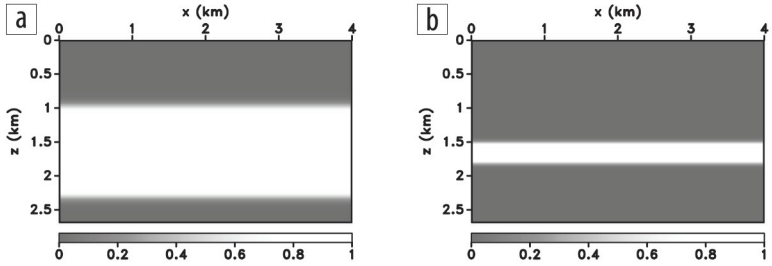

Figure 8. Masks for the model in Figure 7 used in the (a) first and (b) second stages of the facies-based FWI.

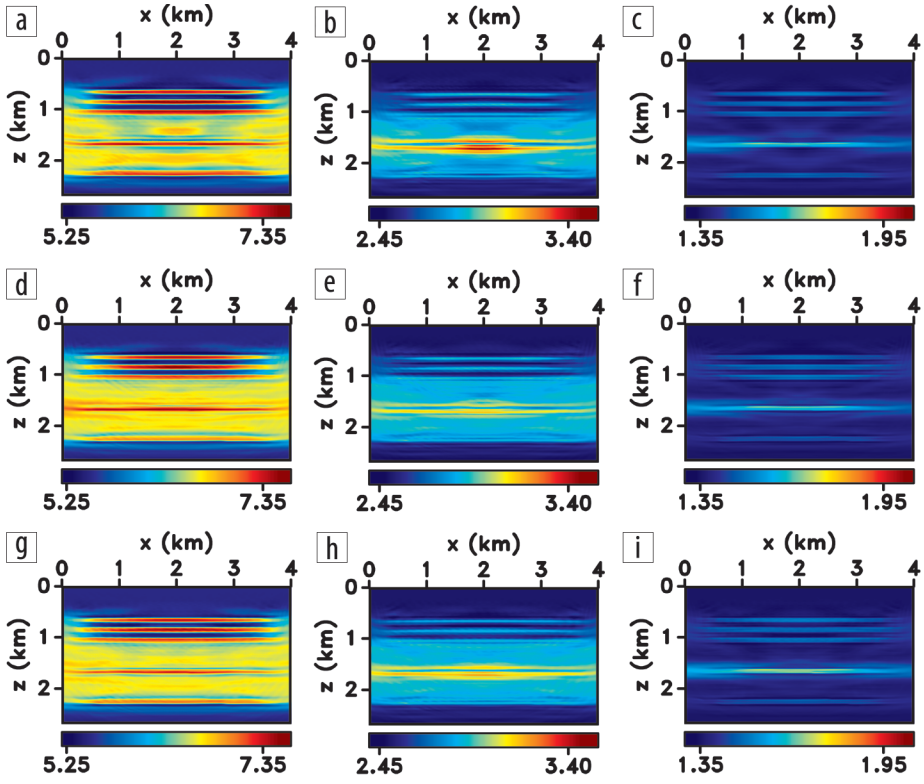

Figure 9. (a) Acoustic impedance I_P and the velocities (b) V_P and (c) V_S for the model from Figure 7 obtained from the standard FWI. The parameters (d) I_P, (e) V_P, and (f) V_S after stage I of the facies-based FWI and (g) I_P, (h) V_P, and (i) V_S after stage II of the facies-based FWI.

The gradient from the data misfit still causes artifacts (although weaker than those obtained from the standard approach) in the inverted η- and ϵ-fields down to a depth of 1 km (Figures 10o and 10p). To eliminate those artifacts, we apply a mask (Figure 8a) to the η- and ϵ-gradients obtained from the data misfit (through the matrix $\mathbf{W}_d$ in equation 1), in addition to the mask employed in the last experiment (Figures 10s and 10t). To increase the contribution of the data misfit, the factor β is about two times smaller than in the previous experiment. Hence, the model-misfit mask $\mathbf{W}_m$ (Figure 8b) penalizes nonzero values of η and ϵ inside the reservoir, while the data-misfit mask $\mathbf{W}_d$ (Figure 8a) mitigates the inversion artifacts in the shallow regions.

Conclusions

With the goal of extending FWI to reservoir-characterization problems, we added facies-based rock-physics constraints through regularization terms in the objective function. The method was first tested on an elastic isotropic model that includes two facies

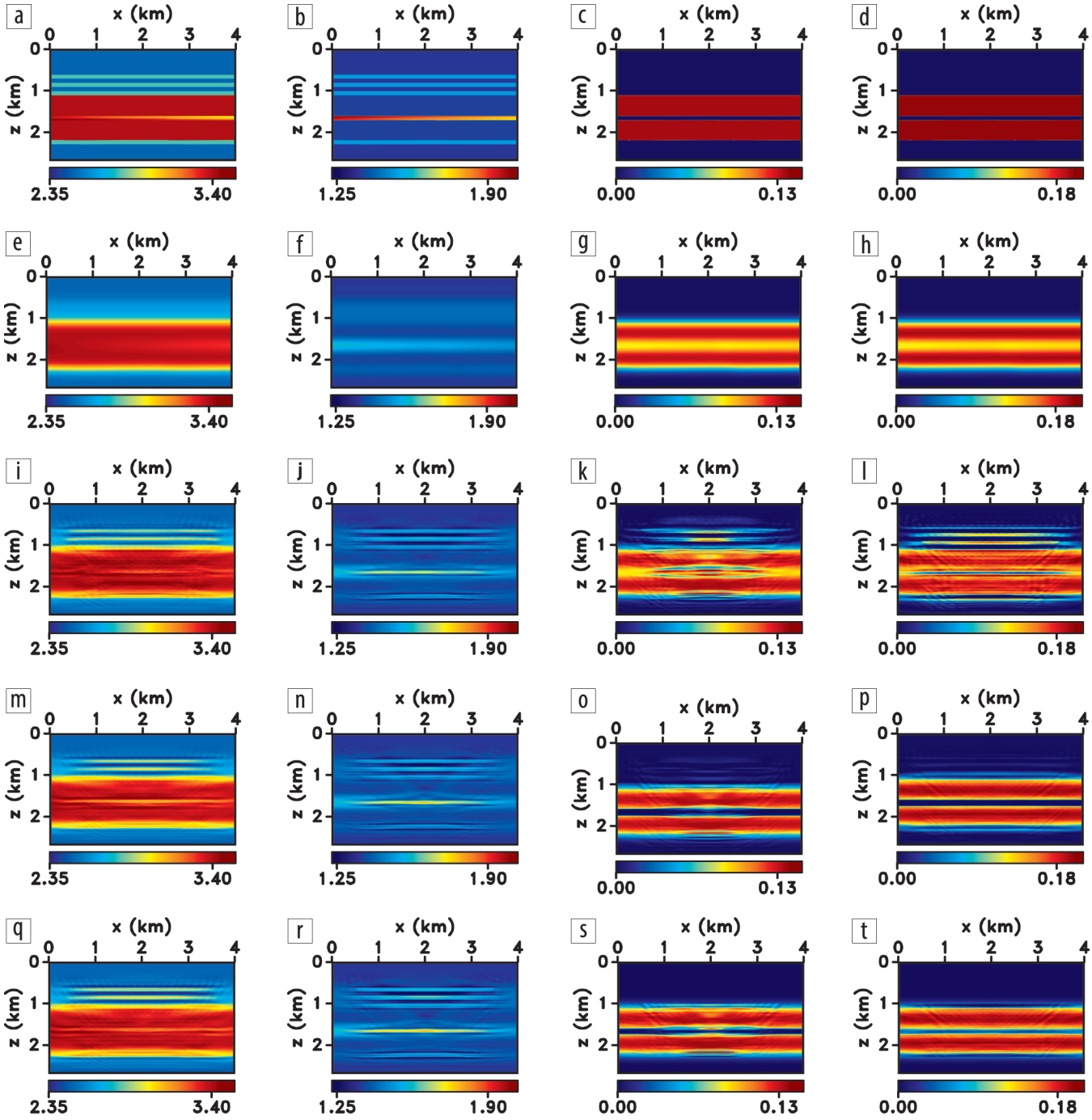

Figure 10. Actual fields of the parameters (a) V_{hor}, (b) V_{S0}, (c) η, and (d) ϵ. The initial parameters (e) V_{hor}, (f) V_{S0}, (g) η, and (h) ϵ. The parameters obtained from the standard FWI: (i) V_{hor}, (j) V_{S0}, (k) η, and (l) ϵ. The parameters obtained from the facies-constrained FWI with the mask in Figure 8b [(m) V_{hor}, (n) V_{S0}, (o) η, and (p) ϵ] and both masks in Figure 8 [(q) V_{hor}, (r) V_{S0}, (s) η, and (t) ϵ].

and is parameterized in terms of the acoustic impedance I_P and the P- and S-wave velocities V_P and V_S. Imposing facies-based constraints during the inversion mitigates artifacts in I_P and improves the resolution in this parameter. The second isotropic model consists of four facies, one of which represents the reservoir. Our algorithm produced more accurate results for the facies encasing the reservoir compared with the standard FWI and improved the resolution in the reservoir parameters.

In another test, we introduced anisotropy in the facies encasing the reservoir (shale). The algorithm updated the P-wave horizontal velocity V_{hor}, the S-wave vertical velocity V_{S0}, and the anisotropy coefficients η and ϵ, while the density field (obtained by smoothing the actual model) was kept fixed. For the chosen parameterization, the objective function is not sufficiently sensitive to η, but the facies-based approach steered the inversion closer to the actual η values by imposing appropriate constraints. To mitigate the artifacts resulting from trade-offs between the P-wave horizontal velocity and the anisotropy coefficients η and ϵ, we applied appropriate constraints to the inversion gradient for the data-misfit term.

Including anisotropy, in addition to making the model more realistic, may represent an advantage (depending on the availability of parameter relationships) for the facies-based algorithm because there are more degrees of freedom in classifying the facies and constraining the inversion. In practice, however, it might be necessary to run a fast-track interpretation or employ probabilistic algorithms to develop facies-based masks that are sufficiently accurate for implementing techniques described in this paper. TLE

Acknowledgments

This work was supported by the Consortium Project on Seismic Inverse Methods for Complex Structures at the Center for Wave Phenomena (CWP) and competitive research funding from the King Abdullah University of Science and Technology (KAUST). We are grateful to Tariq Alkhalifah (KAUST) and Antoine Guitton (CWP) for fruitful discussions. The reproducible numerical examples are generated with the Madagascar open-source software package freely available from www.ahay.org.

Corresponding author: nishant.kamath@univ-grenoble-alpes.fr

References

Alkhalifah, T., and R. Plessix, 2014, A recipe for practical full-waveform inversion in anisotropic media: An analytical parameter resolution study: Geophysics, **79**, no. 3, R91–R101, https://doi.org/10.1190/geo2013-0366.1.

Asnaashari, A., R. Brossier, S. Garambois, F. Audebert, P. Thore, and J. Virieux, 2013, Regularized seismic full waveform inversion with prior model information: Geophysics, **78**, no. 2, R25–R36, https://doi.org/10.1190/geo2012-0104.1.

Byrd, R. H., P. Lu, J. Nocedal, and C. Zhu, 1995, A limited memory algorithm for bound constrained optimization: SIAM Journal on Scientific Computing, **16**, no. 5, 1190–1208, https://doi.org/10.1137/0916069.

Coléou, T., F. Allo, R. Bornard, J. Hamman, and D. Caldwell, 2005, Petrophysical seismic inversion: 75th Annual International Meeting, SEG, Expanded Abstracts, 1355–1358, https://doi.org/10.1190/1.2147938.

Duan, Y., and P. Sava, 2016, Elastic wavefield tomography with physical model constraints: Geophysics, **81**, no. 6, R447–R456, https://doi.org/10.1190/geo2015-0508.1.

Kamath, N., and I. Tsvankin, 2016, Elastic full-waveform inversion for VTI media: Methodology and sensitivity analysis: Geophysics, **81**, no. 2, C53–C68, https://doi.org/10.1190/geo2014-0586.1.

Kamath, N., I. Tsvankin, and E. D'ıaz, 2016, Elastic FWI for VTI media: A synthetic parameterization study: 86th Annual International Meeting, SEG, Expanded Abstracts, 301–305, https://doi.org/10.1190/segam2016-13820100.1.

Operto, S., Y. Gholami, V. Prieux, A. Ribodetti, R. Brossier, L. Metivier, and J. Virieux, 2013, A guided tour of multiparameter full-waveform inversion with multicomponent data: From theory to practice: The Leading Edge, **32**, no. 9, 1040–1054, https://doi.org/10.1190/tle32091040.1.

Plessix, R., 2006, A review of the adjoint-state method for computing the gradient of a functional with geophysical applications: Geophysical Journal International, **167**, no. 2, 495–503, https://doi.org/10.1111/j.1365-246X.2006.02978.x.

Russell, B. H., 1988, Introduction to seismic inversion methods: SEG, https://doi.org/10.1190/1.9781560802303.

Saussus, D., and M. Sams, 2012, Facies as the key to using seismic inversion for modelling reservoir properties: First Break, **30**, no. 7, 45–52, https://doi.org/10.3997/1365-2397.2012009.

Zabihi Naeini, E., T. Alkhalifah, I. Tsvankin, N. Kamath, and J. Cheng, 2016, Main components of full-waveform inversion for reservoir characterization: First Break, **34**, 37–48.

Zabihi Naeini, E., N. Kamath, and I. Tsvankin, 2017, Full waveform inversion for reservoir characterization — A synthetic study: 79th Conference and Exhibition, EAGE, Extended Abstracts, https://doi.org/10.3997/2214-4609.201701246.

Zhang, Z., E. Zabihi Naeini, and T. Alkhalifah, 2017, Facies constrained elastic full waveform inversion: 79th Conference and Exhibition, EAGE, Extended Abstracts, https://doi.org/10.3997/2214-4609.201700719.